Available online at www.sciencedirect.com
SCIENCE DIRECT
Journal of Catalysis 234 (2005) 256–267
JOURNAL OF CATALYSIS
www.elsevier.com/locate/jcat

Behavior of homogeneous and immobilized zinc-based catalysts in cycloaddition of CO_2 to propylene oxide

Michael Ramin, Jan-Dierk Grunwaldt, Alfons Baiker *

Department of Chemistry and Applied Biosciences, Swiss Federal Institute of Technology, ETH Hönggerberg, CH-8093 Zürich, Switzerland

Received 19 January 2005; revised 26 May 2005; accepted 24 June 2005

Available online 9 August 2005

Abstract

Homogeneous and heterogeneous zinc-based catalysts were tested in the reaction of propylene oxide and CO_2 to propylene carbonate without the use of additional solvents. For the preparation of the heterogeneous catalysts, the homogeneous zinc pyridine bromide and acetate complexes were modified for chemical anchoring on a silica surface. All intermediate stages of the series, starting with the zinc pyridine-based complex and ending with the anchored complex, were catalytically tested and characterized. Rates in terms of turnover frequencies (TOFs) > 1100 h^{-1} were obtained with the homogeneous zinc pyridine bromide-based catalysts, and TOFs of 330 h^{-1} were obtained with the corresponding heterogeneous catalyst. Using acetate instead of bromide as a ligand significantly decreased the performance. The differences in activity could be traced to structural differences unraveled by X-ray absorption spectroscopy (XAS). For the heterogeneous catalysts, special attention was paid to the deactivation behavior and the reusability. The catalyst structures were followed in situ by XAS using a specially designed batch reactor cell. This provided important information on the fate of zinc and bromide under reaction conditions and also gave new insight into the reaction mechanism.

Keywords: CO_2 fixation; Cycloaddition; Propylene oxide; Supercritical CO_2; Propylene carbonate; High pressure in situ EXAFS; Deactivation; Zinc pyridine-based catalyst

1. Introduction

Using CO_2 as an environmentally benign, safe, and cheap C_1 building block in synthetic chemistry is a great challenge in "green chemistry" [1,2]. CO_2 is a promising alternative to toxic substances, such as CO and phosgene [3]. Particularly attractive is the application of heterogeneous catalysts in a "solventless" continuous process [4]. Here "solventless" reflects the fact that CO_2 acts not only as a reactant, but also as a solvent. This approach is also attractive because CO_2 is easily separable, nonflammable, nontoxic, and readily available in high purity. In addition, it is in a supercritical state at rather moderate conditions. A promising reaction for the direct fixation of CO_2 into an organic compound is the synthesis of cyclic carbonates like propylene carbonate (4-methyl-[1,3]dioxolan-2-one). These carbonates are used as aprotic solvents for such applications as lithium batteries, polyurethanes, resins, extractions, cleaning, cosmetics, and personal care. Propylene carbonate is also an interesting intermediate for polycarbonates or other polymers [5].

Current industrial processes for propylene carbonate synthesis from propylene oxide (methyloxirane) and CO_2 use alkali metals or bromide as catalysts and ethylene glycol as solvent [6]. The high substrate/catalyst ratio of 1/100 and the substitution of glycols or other solvents by CO_2 (acting as reactant and solvent) motivated several groups to search for alternative catalyst systems. Alkali metal salts with crown ethers or ammonium compounds [7–9], halides of group IV–VI elements, or transition metals with nitrogen or phosphorus containing co-catalysts [10–17], complex multimetal catalysts [18], and catalyst systems involving ionic liquids [19] have been reported.

* Corresponding author. Fax: +41-1-632-11-63.
E-mail address: alfons.baiker@chem.ethz.ch (A. Baiker).

0021-9517/$ – see front matter
doi:10.1016/j.jcat.2005.06.020

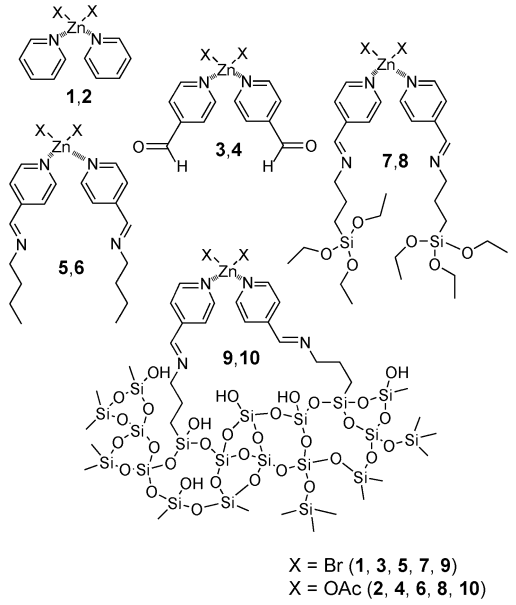

Scheme 1. Series of used zinc complexes. (Complexes designated by an odd number X = Br, complexes designated by an even number X = OAc.)

But for an environmentally benign process, heterogeneous catalysts rather than homogeneous catalysts would be preferable. Hence in recent years various heterogeneous catalysts, including smectite [20], lanthanide oxychloride [21], Mg–Al mixed oxides [22,23], zeolites with encapsulated alkali metals, and aluminum phthalocyanine complexes [24,25], have been investigated. Unfortunately, the catalytic activity of these heterogeneous catalysts is rather low, and a significant gap in performance exists between homogeneous and heterogeneous catalysts. Moreover, studies of the stability and recycling ability of heterogeneous catalysts in the cycloaddition of CO_2 to propylene oxide are rare.

The aim of this study was to investigate the performance of a catalyst step by step from a homogeneous catalyst to its immobilized counterpart. For this purpose, we started from simple and well-performing zinc pyridine bromide complexes and immobilized them according to Scheme 1. The materials were tested for CO_2 fixation and characterized by extended X-ray absorption fine structure (EXAFS), thermoanalysis, and inductively coupled plasma optical emission spectroscopy (ICP-OES). Special emphasis was laid on the immobilized catalyst with respect to structure, deactivation, and reaction mechanism.

2. Experimental

2.1. Materials

The synthesis of the complexes summarized in Scheme 1 used the following materials: 3-aminopropyltriethoxysilane (99%, Acros Organics), 4-pyridinecarboxaldehyde (98%, Acros Organics), *tert*-butylbenzene (+98%, Aldrich), and silica as silicagel 60 (Fluka), all used as received. Propylene oxide (Fluka), *n*-butylamine (Acros), ethanol, pyridine, dichloromethane, chloroform, and diethyl ether were of spectroscopic grade. Zinc bromide and acetate were purchased from ABCR and Acros, respectively. CO_2 4.5 was supplied by Pangas.

2.2. Syntheses of homogeneous catalysts

Catalysts **1**, **2**, **3**, and **4** were prepared as described previously [15]. To a suspension of $ZnBr_2$ (1.126 g, 5.0 mmol) in 40 ml CH_2Cl_2, 2 eq. of pyridine (0.788 g, 10.0 mmol) or 4-pyridinecarboxaldehyde (1.070 g, 10.0 mmol) were added, resulting in complexes **1** and **3**, respectively. For the corresponding zinc acetate catalysts **2** and **4**, zinc acetate (917.4 mg, 0.005 mol) was used instead of zinc bromide. The suspension was stirred overnight at room temperature, then the solution was concentrated and the white precipitate filtrated. The remained traces of pyridine were removed by heating the white crystals under vacuum.

Catalysts **5**, **6**, **7**, and **8** were prepared in the following manner. 4-Pyridinecarboxaldehyde (0.788 g, 10.0 mmol) was added to a solution of *n*-butylamine (0.731 g, 10.0 mmol) or 3-aminopropyltriethoxysilane (2.214 g, 10.0 mmol) in 20 ml CH_2Cl_2. The spontaneously formed yellow imine was stirred for 2 h at room temperature. Then $ZnBr_2$ (1.126 g, 5.0 mmol) was added, and the reaction mixture was stirred overnight. Zinc acetate instead of $ZnBr_2$ was added for synthesis of catalysts **6** and **8**. Subsequent steps were as described earlier.

Ligand characterization of catalysts **5** and **6** was as follows: ^{1}H NMR (500 MHz, $CDCl_3$, TMS): $\delta = 0.96$ [t, ^3J(H,H) = 7.4 Hz, 3H; CH_3], 1.40 (m, 2H, CH_3–CH_2), 1.70 (m, 2H, NCH_2–CH_2), 3.66 [dt, ^2J(H,H) = 1.2 Hz, ^3J(H,H) = 6.9 Hz, 2H, N–CH_2], 7.58 [d, ^3J(H,H) = 4.4 Hz, 2H, 3,5-pyridyl], 8.26 (s, 1H, CH=N), and 8.68 [d, ^3J(H,H) = 4.4 Hz, 2H, 2,6-pyridyl].

Ligand characterization of catalysts **7** and **8** was as follows: ^{1}H NMR (500 MHz, $CDCl_3$, TMS): $\delta = 0.68$ [t, ^3J(H,H) = 8.4 Hz, 2H; CH_2–Si], 1.23 [t, ^3J(H,H) = 7.0 Hz, 9H; CH_3], 1.85 [tt, ^3J(H,H) = 6.9 Hz, ^3J(H,H) = 8.4 Hz, 2H, NCH_2–CH_2], 3.67 [dt, ^2J(H,H) = 1.3 Hz, ^3J(H,H) = 6.9 Hz, 2H, N–CH_2], 3.83 [q, ^3J(H,H) = 7.0 Hz, 6H, O–CH_2], 7.59 [d, ^3J(H,H) = 4.4 Hz, 2H, 2,6-pyridyl], 8.26 (s, 1H, CH=N), and 8.67 [d, ^3J(H,H) = 4.4 Hz, 2H, 3,5-pyridyl].

Results of the elemental analyses were as follows:

*Catalyst **1*** Theoretical values ($C_{10}H_{10}Br_2N_2Zn$): C 31.33%, H 2.63%, N 7.31%; obtained values: C 31.41%, H 2.59%, N 7.28%.

*Catalyst **3*** Theoretical values ($C_{12}H_{10}Br_2N_2O_2Zn$): C 32.80%, H 2.29%, N 6.38%; obtained values: C 32.79%, H 2.29%, N 6.36%.

*Catalyst **5*** Theoretical values ($C_{20}H_{28}Br_2N_4Zn$): C 43.70%, H 5.13%, N 10.19%; obtained values: C 43.77%, H 5.02%, N 10.08%.

Catalyst ***7*** Theoretical values ($C_{30}H_{52}Br_2N_4O_6Si_2Zn$): C 42.59%, H 6.19%, N 6.62%; obtained values: C 42.83%, H 6.11%, N 6.91%.

Results of the nuclear magnetic resonance (NMR) data were as follows:

Catalyst ***1*** ^{1}H NMR (500 MHz, [D$_6$]DMSO, 25 °C): δ = 7.44 (m, 4H, 3,5-pyridyl), 7.84 (m, 2H, 4-pyridyl), 8.59 (m, 4H, 2,6-pyridyl); ^{13}C NMR (500 MHz, [D$_6$]DMSO, 25 °C): δ = 124.7 (4C, 3,5-pyridyl), 138.1 (2C, 4-pyridyl), 148.9 (4C, 2,6-pyridyl).

Catalyst ***2*** ^{1}H NMR (500 MHz, [D$_6$]DMSO, 25 °C): δ = 1.80 (s, 6H, CH_3), 7.40 (m, 4H, 3,5-pyridyl), 7.80 (m, 2H, 4-pyridyl), 8.58 (m, 4H, 2,6-pyridyl); ^{13}C NMR (500 MHz, [D$_6$]DMSO, 25 °C): δ = 22.4 (2C, *C*H$_3$), 124.7 (4C, 3,5-pyridyl), 138.4 (2C, 4-pyridyl), 149.1 (4C, 2,6-pyridyl), 177.1 (2C, *C*OO).

Catalyst ***3*** ^{1}H NMR (500 MHz, [D$_6$]DMSO, 25 °C): δ = 7.82 [d, ^3J(H,H) = 5.9 Hz, 4H, 3,5-pyridyl], 8.89 [d, ^3J(H,H) = 5.9 Hz, 4H, 2,6-pyridyl], 10.10 (s, 2H, C*H*O); ^{13}C NMR (500 MHz, [D$_6$]DMSO, 25 °C): δ = 122.4 (4C, 3,5-pyridyl), 141.6 (2C, 4-pyridyl), 150.8 (4C, 2,6-pyridyl), 193.1 (2C, *C*HO).

Catalyst ***4*** ^{1}H NMR (500 MHz, [D$_6$]DMSO, 25 °C): δ = 1.83 (s, 6H, CH_3), 7.87 [d, ^3J(H,H) = 4.4 Hz, 4H, 3,5-pyridyl], 8.89 [d, ^3J(H,H) = 4.4 Hz, 4H, 2,6-pyridyl], 10.11 (s, 2H, C*H*O); ^{13}C NMR (500 MHz, [D$_6$]DMSO, 25 °C): δ = 22.4 (2C, *C*H$_3$), 122.4 (4C, 3,5-pyridyl), 141.6 (2C, 4-pyridyl), 150.9 (4C, 2,6-pyridyl), 177.0 (2C, *C*OO), 193.1 (2C, *C*HO).

Catalyst ***5*** ^{1}H NMR (500 MHz, [D$_6$]DMSO, 25 °C): δ = 0.92 [t, ^3J(H,H) = 7.5 Hz, 6H, CH$_2$–CH_3], 1.35 (tq, 4H, CH$_3$–CH_2), 1.62 (tt, 4H, N–CH$_2$–CH_2), 3.64 [t, ^3J(H,H) = 6.9 Hz, 4H, N–CH_2], 7.77 [d, ^3J(H,H) = 6.0 Hz, 4H, 3,5-pyridyl], 8.42 (s, 2H, C*H*N), 8.71 [d, ^3J(H,H) = 6.0 Hz, 4H, 2,6-pyridyl]; ^{13}C NMR (500 MHz, [D$_6$]DMSO, 25 °C): δ = 13.7 (2C, CH$_2$–*C*H$_3$), 19.8 (2C, CH$_3$–*C*H$_2$), 32.2 (2C, N–CH$_2$–*C*H$_2$), 60.2 (2C, N–*C*H$_2$), 122.1 (4C, 3,5-pyridyl), 143.5 (2C, 4-pyridyl), 149.9 (4C, 2,6-pyridyl), 159.0 (2C, *C*HN).

Catalyst ***6*** ^{1}H NMR (500 MHz, [D$_6$]DMSO, 25 °C): δ = 0.91 [t, ^3J(H,H) = 7.5 Hz, 6H, CH$_2$–CH_3], 1.34 (tq, 4H, CH$_3$–CH_2), 1.62 (tt, 4H, N–CH$_2$–CH_2), 1.83 (s, 6H, COOCH_3), 3.63 [t, ^3J(H,H) = 6.9 Hz, 4H, N–CH_2], 7.72 [d, ^3J(H,H) = 4.5 Hz, 4H, 3,5-pyridyl], 8.40 (s, 2H, C*H*N), 8.68 [d, ^3J(H,H) = 4.5 Hz, 4H, 2,6-pyridyl]; ^{13}C NMR (500 MHz, [D$_6$]DMSO, 25 °C): δ = 13.7 (2C, CH$_2$–*C*H$_3$), 20.0 (2C, CH$_3$–*C*H$_2$), 22.4 (2C, COO–*C*H$_3$), 32.4 (2C, N–CH$_2$–*C*H$_2$), 60.4 (2C, N–*C*H$_2$), 122.3 (4C, 3,5-pyridyl), 143.9 (2C, 4-pyridyl), 150.0 (4C, 2,6-pyridyl), 159.0 (2C, *C*HN), 177.4 (2C, *C*OO).

Catalyst ***7*** ^{1}H NMR (500 MHz, [D$_6$]DMSO, 25 °C): δ = 0.61 [t, ^3J(H,H) = 8.3 Hz, 4H, CH_2–Si], 1.15 [t, ^3J(H,H) = 7.0 Hz, 18H, CH_3], 1.72 (tt, 4H, CH_2–CH$_2$–Si), 3.63 [t, ^3J(H,H) = 6.4 Hz, 4H, N–CH_2], 3.76 [q, ^3J(H,H) = 7.0 Hz, 12H, O–CH_2], 7.76 [d, ^3J(H,H) = 6.0 Hz, 4H, 3,5-pyridyl], 8.40 (s, 2H, C*H*N), 8.70 [d, ^3J(H,H) = 6.0 Hz, 4H, 2,6-pyridyl]; ^{13}C NMR (500 MHz, [D$_6$]DMSO, 25 °C): δ = 7.5 (2C, *C*H$_2$–Si), 18.2 (6C, *C*H$_3$), 23.8 (2C, *C*H$_2$–CH$_2$–Si), 57.6 (6C, O–*C*H$_2$), 63.0 (2C, N–*C*H$_2$), 122.0 (4C, 3,5-pyridyl), 143.3 (2C, 4-pyridyl), 150.0 (4C, 2,6-pyridyl), 159.3 (2C, *C*HN).

Catalyst ***8*** ^{1}H NMR (500 MHz, [D$_6$]DMSO, 25 °C): δ = 0.62 [t, ^3J(H,H) = 8.4 Hz, 4H, CH_2–Si], 1.17 [t, ^3J(H,H) = 7.0 Hz, 18H, CH$_2$–CH_3], 1.74 (tt, 4H, CH_2–CH$_2$–Si), 1.87 (s, 6H, COO–CH_3), 3.63 [t, ^3J(H,H) = 6.4 Hz, 4H, N–CH_2], 3.77 [q, ^3J(H,H) = 7.0 Hz, 12H, O–CH_2], 7.77 [d, ^3J(H,H) = 6.1 Hz, 4H, 3,5-pyridyl], 8.41 (s, 2H, C*H*N), 8.71 [d, ^3J(H,H) = 6.1 Hz, 4H, 2,6-pyridyl]; ^{13}C NMR (500 MHz, [D$_6$]DMSO, 25 °C): δ = 7.6 (2C, *C*H$_2$–Si), 18.2 (6C, *C*H$_3$), 22.4 (2C, COO–*C*H$_3$), 23.9 (2C, *C*H$_2$–CH$_2$–Si), 57.7 (6C, O–*C*H$_2$), 63.2 (2C, N–*C*H$_2$), 122.1 (4C, 3,5-pyridyl), 143.6 (2C, 4-pyridyl), 150.1 (4C, 2,6-pyridyl), 159.3 (2C, *C*HN), 177.1 (2C, *C*OO).

2.3. Synthesis of immobilized catalysts

The immobilized catalysts **9** and **10** were synthesized by two different procedures, in one approach, the complete complex was synthesized before immobilization (variant I) [26]. For this, silica (3 g) was added to a solution of catalyst **7** or **8** (2.5 mmol) in 40 ml ethanol. The suspension was stirred overnight, filtrated, and washed three times with ethanol, then three times with diethyl ether, and finally dried under vacuum. A second approach (variant II) began with the immobilization of the ligands, followed by the addition of zinc, as described previously [27]. The ligand was built up on the silica surface by immobilization of 3-aminopropyltriethoxysilane (4.43 g, 20.0 mmol) on silica (8 g), denoted by SiO$_2$-mod. For this purpose, the ligand and the support were dissolved/suspended in 100 ml $CHCl_3$ and stirred for 20 h, and then the modified silica was filtered off and washed with ethanol. To a suspension of the modified silica (2 g) in 30 ml ethanol, catalyst **3** (1.4 mmol) was added and treated as described earlier. Only variant I was used for the synthesis of catalyst **10** (starting from catalyst **8**) and the adsorption of catalyst **5** on silica.

2.4. General analysis

Thermal analytical investigations were performed on a NETZSCH STA 409. The samples were heated to 800 °C in a gas stream of 20 vol% O_2 in He. A quadrupole mass spec-

trometer (QMC 420, Balzers) was used to detect the formation of CO_2 and H_2O (traces $m/e = 44$ and 18, respectively). After heating, a known pulse of CO_2 was injected into the sample chamber to calibrate the area of the $m/e = 44$ signal. This calibration enabled calculation of the sample's carbon content. The mass losses of the samples were monitored during the measurements. The zinc and bromide contents of the heterogeneous catalysts **9** and **10** were measured by ICP-OES at ALAB AG (Urdorf, Switzerland).

2.5. CO_2 fixation

The coupling of CO_2 and propylene oxide was done in a 250-ml high-pressure stainless steel autoclave (HPM-P, Medimex). To measure the amount of used CO_2, the entire reactor system was placed on a balance (Toledo IP5 multirange, Mettler). The temperature was controlled by a Eurotherm 900 EPC thermostat. The reaction mixture was stirred by a mechanical stirrer of type EMOD EEDF 56L/2A; the stirring rate was always 1000 min^{-1}. Typically, propylene oxide and the corresponding catalyst were first poured into the reactor. Then the reactor was flushed with CO_2 with the aid of a compressor (PM-101, NWA). A quantity of CO_2 was pressed into the reactor, followed by heating to 140 °C and stirring of the reaction mixture. After a specified reaction time, the reactor was cooled to room temperature, and CO_2 was released by opening the outlet valve. This decompression was done very slowly over a 30-min period. *tert*-Butylbenzene was added to the reaction mixture as an internal standard, and the compounds were analyzed with a gas chromatograph (HP-6890) equipped with a HP-FFAP capillary column (30 m × 0.32 mm × 0.25 µm) and a flame ionization detector. Products were identified by gas chromatography (HP-6890) coupled with mass selective detection (HP-5973) and reference chemicals. As co-products, only propylene glycol and dipropylene glycols were found.

For the leaching tests, the heterogeneous catalyst **9** was separated from the reaction mixture by filtration, washed with diethyl ether, and then dried under vacuum. The used catalyst was applied as described earlier. To detect the catalyst, which was dissolved in the liquid reaction phase, propylene oxide was added to the used and filtrated reaction mixture, which was analyzed before the reaction by gas chromatography and filled in the reactor without further addition of catalyst. Then the reaction was performed as for the other catalytic reactions.

2.6. X-Ray absorption spectroscopy

Ex situ characterization was performed by X-ray absorption near-edge structure (XANES) and EXAFS spectroscopy at the Swiss Norwegian Beamline (SNBL) at ESRF and beamline X1 at HASYLAB. For these experiments, the catalysts were pressed to pellets with polyethylene as additive or placed in thin (1.0-mm diameter) quartz capillaries (Hilgenberg). In addition, in situ experiments were carried out in a batch reactor equipped with a PEEK (polyetheretherketone) container and two beryllium windows. These windows allow investigation of the solid catalyst through a bottom window (1 mm height) and investigation of the liquid phase through an upper window (10 mm above the bottom) [28]. The 10-ml in situ cell can withstand pressure up to 250 bar and temperature up to 200 °C. The reactor is equipped with a magnetic stirrer, inlet and outlet, burst plate (190 bar), and thermocouple. The CO_2 content was measured with a Rheonik mass flow controller. For the experiment, a pellet was placed at the bottom in an upright position. After the first X-ray absorption spectroscopy (XAS) spectrum was obtained, CO_2 was added and the next spectra were recorded. Then the CO_2 was removed and 3 ml of propylene oxide was filled in the cell. During continuous monitoring by EXAFS, CO_2 (7 g) was added once again, and the reactor was heated to 140 °C. The raw data were energy-calibrated (except for the in situ experiments with a too low zinc or bromide concentration), background-corrected, and normalized using WINXAS 3.0 software [29]. After the $\chi(k)$ function was extracted from the EXAFS data, Fourier transformation was performed on the k^1-weighted data in the interval $k = 3.5$–14.0 $Å^{-1}$. Data analysis in the R-space was performed using Zn–Br and Zn–O/N shells calculated by FEFF 6.0 [30]. Only the first coordination shells were used for the fittings. In contrast to the bond length (±0.02 Å), determination of the coordination numbers is not as accurate, and deviations of ±1 could appear.

3. Results

3.1. General catalyst characterization

The preparation of catalysts **1**–**10** was checked in different steps of the synthesis. The chemical composition of catalysts **1** and **3** was identified by accordance between the theoretical value and the results of the elemental analysis. The successful synthesis of the pyridine-based ligands for catalysts **5**–**8** was corroborated by ^{1}H NMR and the measured values (see Experimental section). The reaction of aminopropyltriethoxysilane and, accordingly, of catalyst **8** with the –OH groups of the silica support to gain SiO_2-mod or catalyst **10** was evidenced by the characteristic signals of the $(SiO)_3Si–CH_2$ group (−67.25 ppm) and the $(SiO)_2(O–H/CH_2)Si–CH_2$ group (−60.32 ppm) in the ^{29}Si NMR-spectra (not given).

Both thermal analysis and ICP-OES were used to characterize the immobilized complexes (Table 1). For this purpose, catalysts **9** and **10** were compared with the 3-aminopropyltriethoxysilane–modified silica SiO_2-mod and catalyst **5**. In thermal analysis, all samples demonstrated a loss of H_2O with a peak maximum at 90 °C. No CO_2 was detected at this temperature. Hence this H_2O stemmed from adsorbed H_2O, not from the combustion of immobilized organic compounds. Only traces of hydrocarbons were found,

Table 1
Analytic results of the immobilized complexes measured by thermal analysis and ICP-OES

Catalyst	H_2O[a,b] (%)	C[a] (%)	Zn[c] (%)	Br[c] (%)
SiO_2-mod	0.9	2.6	–	–
5[d]	1.2	0.7	1.3	0.7
9[e]	1.8	1.4	1.5	3.2
9[e,f]	–	–	1.3	1.9
9[g]	0.7	3.9	1.8	7.8
9[g,f]	–	–	1.4	3.0
9[g,h]	–	–	1.3	2.9
9[g,i]	–	–	1.4	4.7
10	1.2	4.7	3.2	–

[a] Measured by thermal analysis.
[b] Content of adsorbed water.
[c] Results of ICP-OES.
[d] Adsorbed complex **5** on silica.
[e] Synthesized by variant I.
[f] After one use.
[g] Synthesized by variant II.
[h] After second use.
[i] After one reuse with additional KBr for catalyst regeneration.

due to incomplete removal of solvents and chemicals after synthesis or to adsorption of hydrocarbons on the silica in the laboratory atmosphere. The H_2O content is also given in Table 1. The carbon content of the immobilized 3-aminopropyltriethoxysilane alone on silica (intermediate step during variant II of catalyst **9**), was 2.6%. CO_2 was formed in two sharp temperature ranges with maxima at 305 and 393 °C (50 °C width), and one broad signal from 360 to 600 °C. The first signal at 305 °C disappeared after the grafting of the pyridine zinc complex leading to sample **9**, and a new strong signal arose at 520 °C. The two sharp signals of the modified silica could originate from different positions of the immobilized aminopropyl group. One of these anchors reacted with the zinc complex; the other may have been sterically hindered by its position on the silica. Catalyst **9** variant I demonstrated hydrocarbon combustion over a broader temperature range with maxima at 432 and 574 °C. No signal due to free aminopropyl groups was discernible at 390 °C. Both catalysts seem thermally rather stable. The higher combustion temperatures of catalyst **9** variant II were caused by changes in the immobilized complex compared with variant I. The same results as for catalyst **9** variant I were obtained for catalyst **10** variant I, except that the second peak was shifted to lower temperatures because of the lower thermal stability of the acetate groups.

In contrast, catalyst **5** on silica exhibited combustion over a very broad temperature range, with a maximum at 465 °C, and the lowest carbon content of all samples. But the zinc content was too high compared with the measured carbon and bromide contents. The covalently anchored complexes in catalysts **9** and **10** had a higher carbon and bromide content than the adsorbed complex in catalyst **5**. A favored coordination of zinc by hydroxyl groups of the silica could explain the higher zinc content. The hydroxyl groups on the silica surface were not blocked by a silylation reaction as

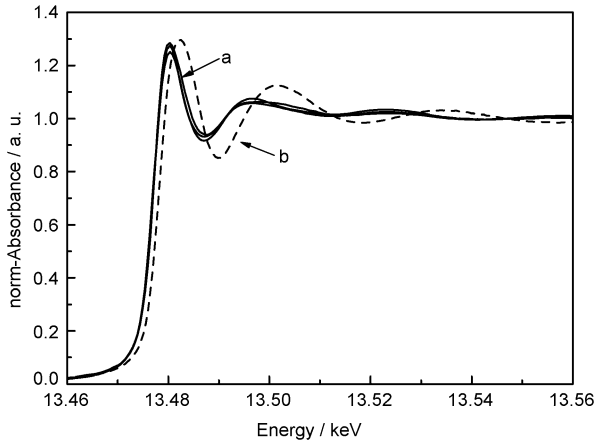

Fig. 1. Ex situ XANES spectra at the Br *K*-edge. (a) catalysts **1**, **7**, and **9**. (b) KBr as reference.

occurred for the chemically bound complexes. The higher carbon content of catalysts synthesized by variant II compared with those synthesized by variant I was likely due to the free aminopropyl groups on the silica surface.

3.2. *Ex situ X-ray absorption measurements*

The XANES region of an X-ray absorption spectrum provides information on the first coordination shell of the excited atom, such as coordination geometry and the oxidation state. Additional structural information can be obtained by EXAFS spectroscopy [31,32]. The postedge region in XAS can provide information on the bond length, coordination number, and nature of scattering atoms around the absorbing center.

The Br *K*-edge XANES spectra of the bromide-containing catalyst series (complexes **1**, **7**, and **9**) (Fig. 1) demonstrated no change in the near-edge region. Hence the local structure of the bromide remained similar during the immobilization series. This finding is supported by the fact that in the spectrum of dissolved KBr, the edge energy and the shape of the Br *K*-edge XANES changed. Small changes indicating a different local structure were seen at the Zn *K*-edge (Fig. 2). In particular, catalysts **3**, **7**, **9**, and **10** exhibited greater absorption at 9668 eV than did catalysts **1** and **5**. The greatest absorbance was seen for catalyst **10**, in which zinc is surrounded by 6 N/O atoms; this seems to lead to the white line and the additional feature at 9.668 keV. Ethoxy groups of the molecule or silanol groups of the silica surface could provide additional coordination via oxygen atoms for catalysts **7** and **9**. Only a small feature at 9.668 keV and a strong white line were seen for catalyst **3**, in which steric reasons hindered an inner molecular oxygen coordination of the zinc. In contrast to the bromide catalysts, a striking white line is missing for the immobilized acetate complex **10**, possibly due to differing symmetries (tetrahedral vs. octahedral) [33].

Figs. 3 and 4 show the extracted Zn *K*-edge EXAFS functions and the corresponding Fourier-transformed k^1-weighted EXAFS spectra at the Zn *K*-edge. The spectra of

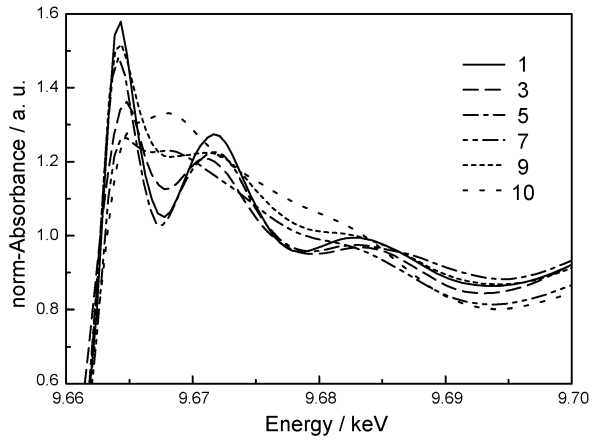

Fig. 2. Ex situ XANES spectra of Zn-complexes **1**, **3**, **5**, **7**, **9**, and **10** at the Zn *K*-edge. The labels of the catalysts correspond to those indicated in Scheme 1.

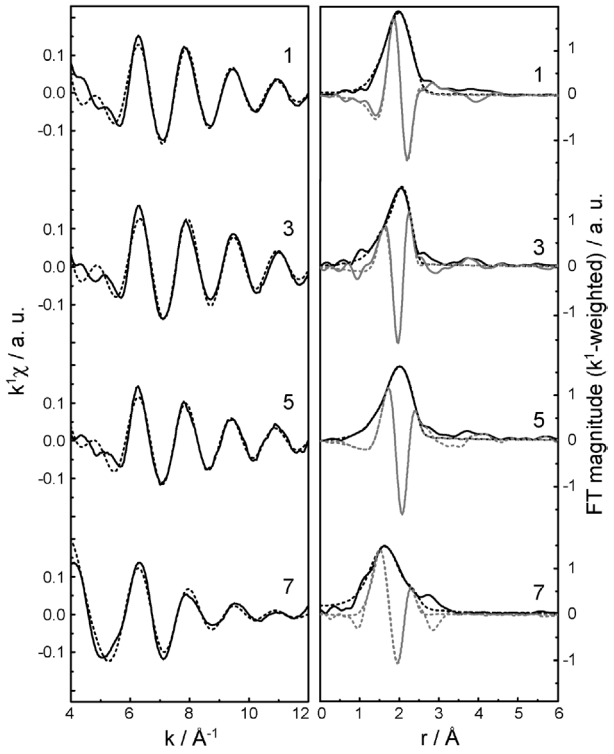

Fig. 3. Experimental and fitted k^1-weighted $\chi(k)$ functions and their Fourier transforms of the different homogeneous complexes **1**, **3**, **5**, **7** at the Zn *K*-edge. Experimental data are shown by solid lines, the fitted data by dotted lines. Grey lines in the right part reflect the imaginary part of the Fourier transform. The labels of the catalysts correspond to those indicated in Scheme 1.

the zinc pyridine-bromide catalysts **1**, **3**, **5**, **7**, and **9** demonstrated contributions from both N and Br. Because of the similar backscattering amplitude of N and O, one cannot differentiate between these two neighbors in the measurements. Zn–Br distances were identical with data for similar zinc pyridine-bromide complexes obtained by X-ray crystallography [15,17], and the bond length was coincident in Fourier-transformed spectra of Zn and Br *K*-edge. The

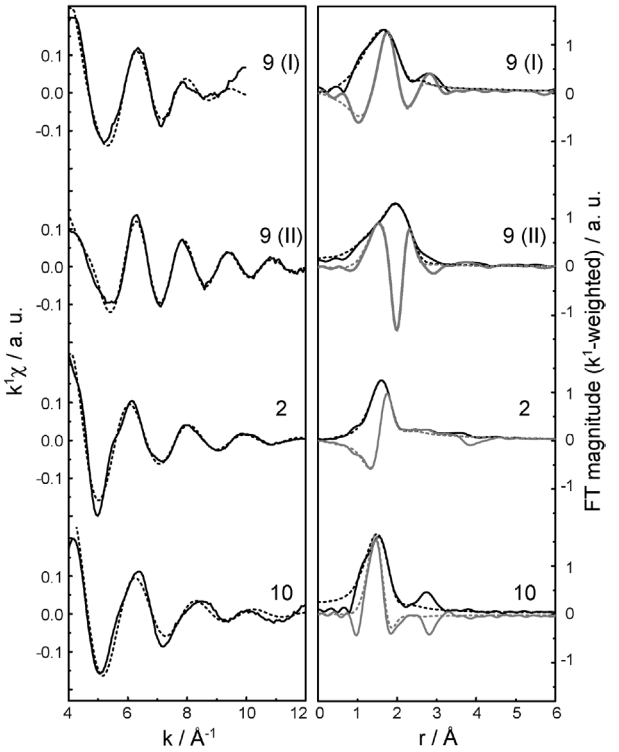

Fig. 4. Comparison of experimental and fitted k^1-weighted $\chi(k)$ functions and their Fourier transforms of heterogeneous bromide and the acetate complexes (Zn *K*-edge). Experimental data are designated by solid lines, calculated by dotted lines. Grey lines in the right part are the imaginary part of the Fourier transform. The numbers are corresponding to the catalysts shown in Scheme 1, 9 (I) is designated for catalyst **9** synthesized by variant I, 9 (II) is catalyst **9** variant II.

structural parameters are given in Table 2. Although it is significant that the ratio of the coordination number of the Br and N/O neighbors is > 1.6 for catalysts **1**, **3**, and **5**, it is about 1 or even < 1 for catalysts **7** and **9**. This finding can be explained by coordination of the zinc atom with oxygen atoms from the ethoxy groups of the molecule or the silanol groups of the surface. Striking differences were also found in the Fourier-transformed spectrum for complex **7** compared with complexes **1** and **5**, indicating a greater number of oxygen and/or nitrogen neighbors. Complex **9** variant I demonstrated higher coordination by oxygen neighbors than variant II. Note that for variant II, the complex was immobilized by reaction with former installed molecules on the silica surface, and that variant I was an immobilized complex **7** exhibiting coordination of the zinc by ethoxy groups. It is possible that only one anchor was used for the immobilization and that the free anchor was coordinating the active center.

3.3. Catalytic performance in CO_2 fixation

The catalytic results from the cycloaddition of CO_2 and propylene oxide to the homogeneous and heterogeneous catalysts are given in Table 3. The difference in activity between the pyridine complex **1** and the modified complex **5** is in-

Table 2
Structural parameters determined from the Zn K-edge and the Br K-edge EXAFS spectra

Catalyst	A[a]–Bs[b]	r[c] (Å)	N[d]	σ^2[e] (Å)	ΔE_0[f] (eV)	Residual[g]	k-Range (Å^{-1})
1	Zn–Br	2.375	2.7	0.006	2.2	5.4	3.5–14.0
	Zn–N	1.985	1.6	0.001	−5.4		
2	Zn–N/O	1.998	3.6	0.006	3.8	1.8	3.5–14.0
3	Zn–Br	2.356	2.9	0.005	0.4	6.0	3.5–14.5
	Zn–N	1.970	1.8	0.003	−9.2		
	Br–Zn	2.347	1.2	0.005	−0.2	7.8	3.5–11.5
5	Zn–Br	2.376	2.8	0.006	1.8	4.3	3.5–14.0
	Zn–N	1.997	1.7	0.004	−2.9		
7	Zn–Br	2.365	3.0	0.008	0.8	6.5	3.5–14.0
	Zn–N/O	1.971	3.4	0.007	5.2		
9[h]	Zn–Br	2.370	2.1	0.015	1.8	3.7	4.0–10.0
	Zn–N/O	1.950	3.2	0.019	−0.6		
9[i]	Zn–Br	2.377	2.7	0.005	−1.1	3.6	3.5–12.0
	Zn–N/O	1.985	2.5	0.003	−2.3		
	Br–Zn	2.375	1.7	0.006	0.9	2.0	3.5–12.0
10	Zn–N/O	1.946	4.7	0.008	4.4	10.8	3.5–12.5

[a] Absorber.
[b] Backscatterer.
[c] Distance.
[d] Coordination number.
[e] Debye–Waller factor.
[f] Shift of the energy threshold.
[g] Quality of fit according to Ref. [29].
[h] Synthesized by variant I.
[i] Variant II.

Table 3
Catalytic results[a]

Catalyst	Y[b] (%)	S[c] (%)	TON[d]	TOF[e] (h^{-1})
1[f]	90.7	99.3	910	228
1	66.7	99.4	3376	1125
2	3.1	86.3	111	37
3	38.2	100.0	1972	657
4	1.3	56.1	46	15
5	62.5	99.5	3165	1055
6	5.6	88.2	200	67
7	42.3	98.5	1979	660
8	2.7	76.2	95	32
5[g,h]	1.4	57.7	39	13
9[g,i]	51.8	98.5	994	331
9[g,j]	18.9	98.2	597	199
10[g,k]	18.1	95.1	209	9
9[g,i,l]	31.9	99.7	862	287
9[g,i,m]	56.3	99.6	1520	507
9[g,i,n]	42.1	71.8	865	288

[a] Reaction was carried out in 10 ml (140 mmol) of propylene oxide, catalyst (0.03 mmol, 0.0002 eq.), CO_2 (480–550 mmol, 3.4–3.9 eq.), reaction time was 3 h at 140 °C.
[b] Yield of propylene carbonate based on propylene oxide.
[c] Selectivity of propylene carbonate.
[d] Turnover number [mol of product (mol of catalyst)$^{-1}$].
[e] Turnover frequency [mol of product (mol of catalyst · h)$^{-1}$].
[f] Catalyst (1.4 mmol, 0.001 eq.), reaction time 4 h.
[g] 250 mg of solid catalyst was used (0.08–0.15 mmol, 0.0006–0.001 eq.).
[h] Adsorbed on silica, the TOF is based on the mol of Zn.
[i] Prepared by variant II.
[j] Prepared by variant I.
[k] Reaction time 24 h.
[l] Used catalyst.
[m] Used catalyst in presence of 0.14 mmol NH_4Br.
[n] Unused catalyst with addition of 73 mmol water.

significant. Interestingly, the activity of catalysts **3** and **7** was significantly lower. Note that the coordination geometry determined by EXAFS for catalyst **7** was different; the coordination number for N/O neighbors was higher. Comparative reactions with the acetate complexes (high N/O coordination number – no bromide) also demonstrate the importance of bromide in this reaction. Lower rates were observed with the heterogeneous catalyst system **9**. This may be due to mass transfer limitations, as discussed later.

The only byproducts were propylene glycol and dipropylene glycols. These always appeared in similar (small) amounts. This results from the residual H_2O in the batch reactor, because the addition of 73 mmol H_2O decreased the selectivity from 99 to 71.8%. However, this also explains the very low selectivity with the adsorbed catalyst **5** on silica. The same experiment also illustrated that it is not sufficient to adsorb a homogeneous catalyst on a surface. Simple washing of the catalyst removed the active component. The low activity of the adsorbed catalyst could be explained by the small amounts of complex **5** that remained adsorbed after preparation. After the first reaction, the reused catalyst exhibited no activity. The low rates in terms of turnover frequency (TOF) of catalyst **5** on silica was due to the relatively high zinc content compared with the carbon and bromide content. The TOF was calculated with zinc considered an active component, and as discussed earlier (Section 3.1), the zinc on this catalyst was coordinated by hydroxyl groups of the silica support. Thus this zinc was not catalytically active.

An important feature of heterogeneous catalysts is their long-time behavior during catalytic runs and, accordingly, their behavior toward deactivation during reuse. Therefore, emphasis was placed on studying leaching of the metal and/or ligand from the support. A simple way to gain insight into this issue is to reuse both solid and liquid phases [34,35].

Fig. 5 shows that reuse of catalyst **9** led to an exponential decrease in activity. Actually, after five repeats, the activity was comparable to that of the fresh catalyst **10** (Fig. 5). Despite this deactivation, however, only low catalytic activity was detected in the liquid phase. This activity corresponds to a loss of about 4.5 µmol of active component in the first use; the second use saw a loss of about 1.5 µmol, calculated with the data of catalyst **7**. But this represents $< 8\%$ of the total amount of the active component and thus cannot explain the deactivation phenomenon. When the catalyst was reused a second time, the liquid phase exhibited no catalytic activity and thus no leaching of an active catalyst. The leaching of active catalyst from the support to the liquid in the first two uses could be explained by the removal of adsorbed species from the silica surface, because the reaction mixture itself is

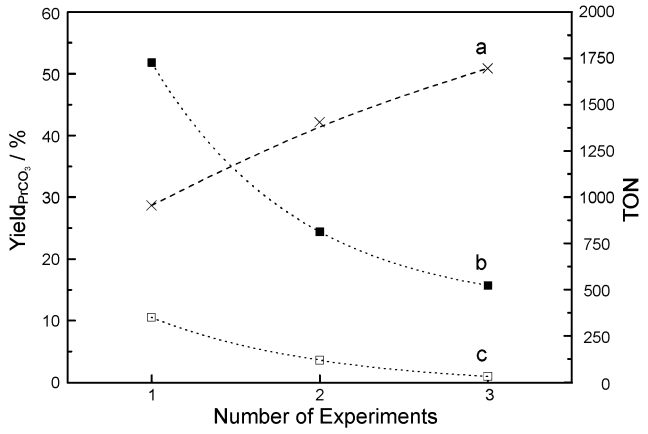

Fig. 5. Deactivation experiments of catalyst **9**. (a) TON summarized over all recycle steps, (b) exponential decrease of the yield of propylene carbonate by re-use of the solid catalyst, (c) yield of the leaching test. The test itself [34,35,40] could not explain this behavior. After the first reuse there is no active catalyst left in the liquid phase.

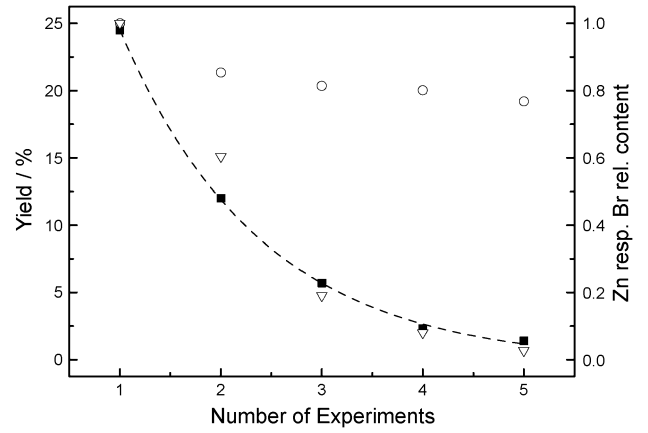

Fig. 6. Deactivation experiments of catalyst **9**. Solid squares are designated to the yield of propylene carbonate. The dashed line is an exponential fit of the decrease. Circles indicate the zinc content and triangles the bromide content, both measured by ICP-OES.

more "aggressive" than the liquid used for washing the synthesized catalyst after preparation. Nevertheless, leaching of the active component could not explain the detected deactivation.

More information of the deactivation mechanism was gained by ICP-OES and XAS measurements of the reused catalyst samples. ICP-OES revealed that the zinc content decreased only slightly during the first experiment (Table 1), whereas bromide was washed out with every further reuse. Thus the decreased bromide content occurred in parallel to the loss of catalyst activity (Fig. 6).

3.4. In situ X-ray absorption measurements

To understand the catalyst structure in more detail under reaction conditions, we monitored the catalyst in situ with XANES and EXAFS spectroscopy. For this purpose, we applied a batch reactor with two Be windows (as described in Experimental section). The lower window was directly over the bottom of the reactor, and the solid catalyst was analyzed through this window. The spectrum of the liquid phase was measured through the upper window. To avoid having a suspension in the liquid phase, stirring was stopped during measurements.

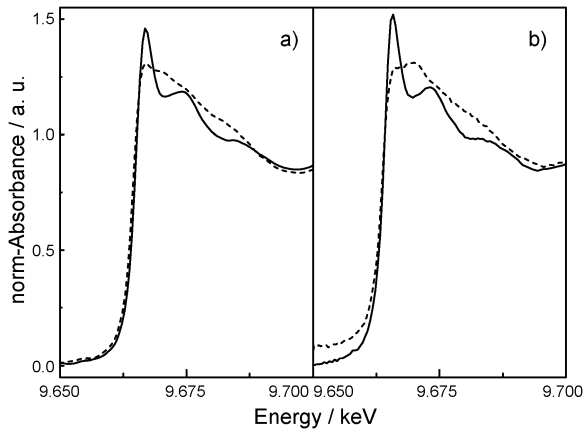

Fig. 7. In situ XANES spectra of catalyst **9** at the Zn *K*-edge. A striking change appeared after the addition of propylene oxide (dashed lines), (a) without carbon dioxide, (b) with carbon dioxide.

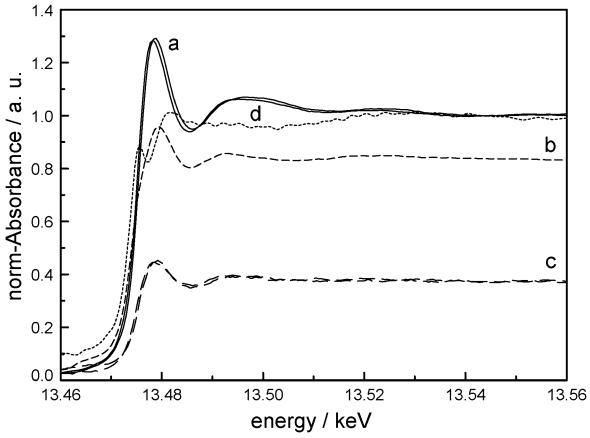

Fig. 8. In situ XANES spectra of catalyst **9** at the Br *K*-edge. The spectra are not normalized with respect to the first spectrum to point out the loss of bromide with the exception of the spectra of the liquid phase, (a) spectra with catalyst as synthesized, (b) after 30 min of addition of propylene carbonate, (c) after 3 h of reaction at 140 °C and after cooling down to ambient temperature, (d) spectrum through the liquid phase during reaction. On the anchored complex no change of the neighbors could be seen, but the bromide detected in the liquid phase had a completely different ligand sphere (normalized).

The XANES spectra at the Zn *K*-edge changed dramatically after propylene oxide was added in a nonreversible manner (Fig. 7). Interestingly, the structural changes were similar regardless of whether or not CO_2 was present. Merely the addition of propylene oxide changed the XANES spectra to be more like the spectra of the bromide-free acetate complex (compare Figs. 7 and 2). No change in the spectrum itself could be seen at the Br *K*-edge, but the edge jump decreased and the signal became increasingly noisy during the reaction (Fig. 8). Also during the reaction, X-ray absorption spectra were recorded for both the liquid phase

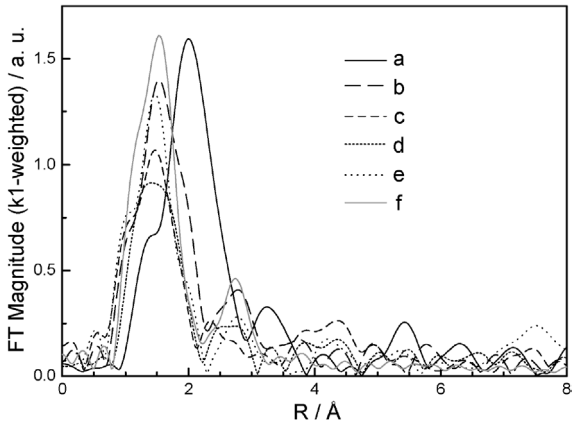

Fig. 9. Fourier transformed in situ EXAFS spectra. Fourier transformed $k^1\chi(k)$ function of catalyst **9** (a). A fast change in the spectra appeared after the addition of propylene oxide (b). The signal corresponding to the bromide is disappearing whereas the signal of N/O atoms becomes more dominant. Addition of carbon dioxide (c) and increase of the temperature to 140 °C during reaction (d) decreased the signal. After the reaction (e) there is no significant difference to the spectrum of the bromide free catalyst **10** (f).

and the solid catalyst. No absorption was found at the Zn *K*-edge in solution, but an intensive signal was detected at the Br *K*-edge. The XANES spectra at the Br *K*-edge were different from those of the bromide in the solid phase (Fig. 8). This finding is reasonable, because although bromide will not dissolve in CO_2, small amounts added to the epoxide could be present in solution. Comparable XANES spectra have been reported for Br–C bonds [36]. Along with the XANES data, the in situ EXAFS experiments at the Zn *K*-edge (solid catalyst) indicate a significant change in the coordination shell of the zinc center (Fig. 9). After a short contact time between the catalyst and propylene oxide, the strong signal at 2 Å in the Fourier-transformed EXAFS spectra at the Zn *K*-edge disappeared. The signal at about 2 Å is typical for the Br backscatterer, demonstrating that Br dissolves. Correspondingly, in the spectra of the solid catalyst at the Br *K*-edge during reaction just a small and hardly interpretable signal remained, also demonstrating the loss of bromide. After the reaction, only the backscattering of N or O neighbors could be detected (Fig. 9), and no Br surrounded the central zinc atom. There was little difference in the EXAFS spectrum at the Zn *K*-edge from catalyst **10**.

In addition, we estimated the bromide concentration in our in situ batch reactor as follows. In the liquid phase (upper part of the reactor), the bromide was calibrated by solutions of known bromide concentration and resulted in a concentration of about 5 mmol l^{-1}. The bromide loss of the catalyst determined by the decrease of the edge jump (the lower part of the reactor) produced a concentration of 15 mmol l^{-1}. This greater amount may be related to a larger-than-expected volume of the liquid phase or to some abrasion of the pellet resulting from mechanical impact caused by the stirring. The difference in the edge jumps before and after the reaction lead to a bromide loss of 55% during reaction; this is less than the drop in bromide content measured by ICP-OES after a standard reaction. But note that a pellet was used for the in situ experiments, and consequently intraparticle mass transfer was less effective compared with the powder.

3.5. Reactivation of the catalyst by bromide addition

Because bromide loss seems to be the main cause of the deactivation of the immobilized catalyst **9**, it should be possible to regenerate the catalyst by reading bromide. Indeed, the addition of both KBr and NH_4Br lead to reactivation of the catalyst (Table 3). An increased Br content was obtained in ICP-OES measurements (Table 1); however, EXAFS measurements showed that the coordination geometry around the zinc central atom was not regenerated. No signal of a backscattering Br neighbor with the typical Zn–Br distance was found. The additional Br on the catalysts was adsorbed on the surface of the silica and was not assembled in the zinc complex; thus regeneration led not to structure **9** of the immobilized catalyst, but rather to bromide as a cocatalyst. This has significant effects on the mechanism.

4. Discussion

4.1. Immobilization and structure of the catalysts

The different analytical methods confirmed successful immobilization of the zinc pyridine complex. The covalent fixation via the silylether groups was indicated by the ^{29}Si NMR spectra. Elemental analysis confirmed the composition of the homogeneous catalysts, and both ICP-OES and thermal analysis identified the composition of the immobilized catalyst **9**. There were no significant changes in the EXAFS spectra of the series toward the immobilized species. Fourier-transformed EXAFS spectra at the Br and Zn *K*-edges, as well as fit results, indicated two different neighbors in the coordination sphere of the zinc atom with distances of 1.98 and 2.37 Å, respectively. The catalysts containing silylether or acetate groups **7**, **9**, and **10** exhibited a tendency toward higher coordination numbers. This may be due to an additional coordination of the oxygen, because XANES indicated a change in geometry and EXAFS revealed variation in the coordination numbers. Usually, a tetrahedral coordination of zinc would be expected; however, small groups like H_2O can lead to a change from a tetrahedral to an octahedral environment. In addition, the ratio of the peak areas of Br and N/O neighbors changed. For catalysts **1**, **3**, and **5**, the bromide contribution was dominant (Fig. 3), but the ethoxy group containing catalyst **7** exhibited more pronounced N/O backscattering compared with the bromide. This finding was also seen for catalyst **9** variant I, which could be regarded as immobilized catalyst **7**. An equal signal contribution demonstrated catalyst **9** variant II. Here it was not possible to coordinate the zinc by the flexible ethoxy groups, because these groups were previously bound to the silica support. Only

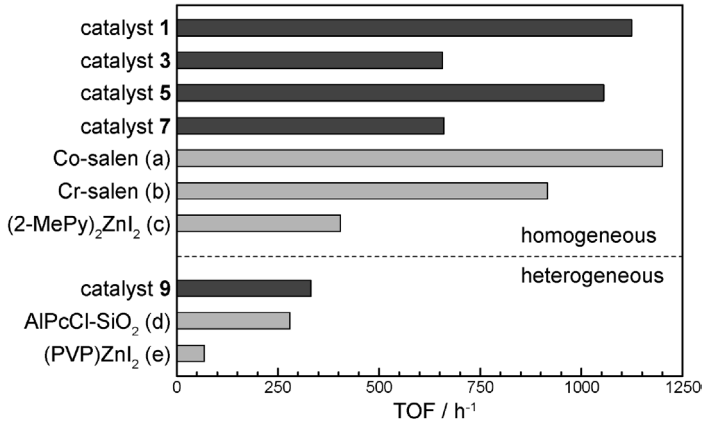

Fig. 10. Comparison of catalysts in this work and other monometallic catalyst for the synthesis of propylene carbonate by carbon dioxide fixation. Dark bars are designated to the catalysts of this work, the bright ones to examples of the literature. (a) Co-salen catalyst with DMAP as Lewis base co-catalyst and CH_2Cl_2 as additional solvent [39], (b) Cr-salen catalysts [14] in presence of CH_2Cl_2, (c) homogeneous zinc catalyst [16], (d) aluminum phthalocyanine complex covalently bonded to MCM-41 silica with *n*-butylammonium bromide as co-catalyst [38], (e) PVP-supported zinc catalyst [37].

the remaining ethoxy groups, short free silanol groups of the surface or even free immobilized pyridine precursors, could coordinate to the zinc center. In the EXAFS spectra, no typical Zn–Zn contributions were found; however, Darensbourg [15] reported not only monomeric zinc pyridine bromide complexes, but also di- and trimeric species coupled by zinc bridges. In summary, the complete series of catalyst from the homogeneous complexes **1** and **2** to the heterogeneous counterparts **9** and **10** could be prepared and the structure of the active center preserved.

4.2. Comparison of the catalytic activity of homogeneous and heterogeneous catalysts

As discussed earlier, our strategy of modifying the pyridine step by step toward an immobilized complex proved successful. The catalytic data demonstrate that each intermediate was catalytically active. This indicates no significant change in the catalytically active center. To our knowledge, this is the first time that the metamorphosis from a homogeneous toward a heterogeneous catalyst for propylene carbonate formation was presented in all steps, allowing us to compare the catalytic results and study the effects of the immobilization process.

The selectivity of these catalysts to propylene carbonate is high, reaching nearly 100%. The formation of trace amounts of polymeric materials, such as polypropylene oxide or polypropylene carbonate, cannot be ruled out. Byproducts detected in low quantities were propylene glycol and dipropylene glycol, which can be explained by traces of H_2O in the reactor and in the ligand sphere of the catalyst or its surface.

The activity of the bromide-containing homogeneous catalyst series is high compared with that of other catalysts in this system [14,16,37–39]. Fig. 10 compares the catalytic data of selected catalysts of this work with those reported in previous studies. TOFs $> 1000\ h^{-1}$ were obtained for catalysts **1** and **5**. The catalytic performance of catalysts **3** and **7** with TOFs $> 600\ h^{-1}$ is high as well. Compared with the highest achieved TOF of $1125\ h^{-1}$ for catalyst **1**, only very recently reported homogeneous salen complexes with co-catalysts are more active (Fig. 10). Note, however, that the very active salen-based catalysts require co-solvents to reach their high performance; for example, Cr-salen catalysts [14] with dichloromethane as an additional solvent yielded a TOF of $916\ h^{-1}$. The same group also reported an improved system (TOF up to $1200\ h^{-1}$) through the use of Co complexes and DMAP as a Lewis base in dichloromethane. Our work aimed to develop a solventless process using CO_2 as both solvent and reactant. The catalytic activity of the homogeneous Zn-based catalysts of this work is also higher than that of comparable catalyst systems reported by Kim et al. [16,17,37]. One reason for this may be the higher reaction temperature in our studies (140 compared with 100 °C). Kim enhanced the performance of these complexes by substituting at the ortho position of the pyridine ring and using iodide instead of bromide. Accordingly, the potential exists to design more powerful catalysts by varying the catalysts of this work. Note also that recently, a complex mixture of different metals and co-catalysts resulted in even higher rates [18].

Focusing on the immobilized catalysts, a three-fold decrease is observed compared with the homogeneous counterparts. Nonetheless, to our knowledge, catalyst **9** prepared by variant II is the most active heterogeneous catalyst for the fixation of CO_2 to propylene carbonate (Fig. 10), allowing a turnover number (TON) of > 5000. Moreover, we see that the gap between homogeneous and heterogeneous catalysts is smaller than has been reported in the literature up to now. He et al. [38] achieved related TOFs with similar selectivity only with an aluminum phthalocyanine complex covalently bonded to MCM-41 silica and *n*-butylammonium bromide as a co-catalyst. Until now, the best system without a co-catalyst was the resin-immobilized zinc iodide complex [37],

but an inorganic support would be more desirable for higher thermal and mechanical stability.

As outlined earlier, EXAFS found no difference in the coordination sphere for catalysts **1**, **3**, and **5**, but catalyst **3** exhibited only half of the activity of the other two catalysts. The basicity of the ligands of these catalysts depends on possible electron-donating and withdrawing groups, and the strength of the Zn–N bond will decrease for the less-basic pyridine ligand [17]. The polarity of the complexes is also important; this is significantly different for catalyst **3**. The poorer performance of catalysts **7** and **9** compared with catalysts **1** and **5** can be explained by the greater coordination of the Zn with ethoxy or silanol groups. The better catalytic performance of the homogeneous catalysts compared with their immobilized counterparts may be due to sterical constraints and decreased accessibility of the latter. Kim et al. [17] investigated the influence of additional pyridine and found decreased activity. They explained this effect as resulting from competition of the added pyridine and propylene oxide for coordination to the zinc center. Thus increased coordination of the active center decreased the catalytic activity of catalysts **7** and **9**.

For catalyst **9**, variant I exhibited poorer performance than the immobilized catalyst synthesized by variant II. The structural studies demonstrated a different structure, probably because complex **9** variant I was completely synthesized before immobilization (immobilized catalyst **7**). One of the anchor side chains caused an additional coordination by oxygen groups, which apparently decreased the activity of the complex.

Hence the structure of the active center needs to be as similar as possible to that of catalyst **1**. Consequently, the activity of the acetate containing catalysts **2**, **4**, **6**, **8**, and **10** was poor compared with that of the bromide-containing catalysts. This finding underlines the important role of Br in the reaction and indicates that a higher coordination of zinc by oxygen atoms hampers the coordination of the propylene oxide to form an active species.

4.3. Behavior of the catalyst under reaction conditions

Important features of heterogeneous catalysts are their deactivation behavior and reusability. In situ EXAFS studies demonstrated that the Zn complex was well immobilized on the support even under reaction conditions. However, a loss of bromide into propylene oxide or a propylene oxide–CO_2 mixture was found that led to deactivation of the catalyst. Interestingly, Kim et al. [37] found no such deactivation; however, their deactivation studies were performed in ethylene oxide instead of propylene oxide. The dissolution of bromide explains the deactivation of the catalyst during reuse, as well as the negative leaching tests. Such tests are usually performed to identify whether the active complex goes into solution [34,35,40]. Because the entire active complex did not leach, no activity was found in the liquid phase. Consequently, the former activity could be recovered by adding bromide to the solid catalyst. Hence in this case, bromide was used as a co-catalyst. Regeneration of the complex (i.e., the coordination of Br to Zn) was not seen on EXAFS.

4.4. Role of bromide

The observation that bromide is dissolved in the liquid phase also has important implications for the mechanism. Kim et al. [17] and He et al. [38,41] proposed mechanisms that first consider either activation of CO_2 or coordination of epoxide by the metal center. These authors found no changes in the bromide after the reaction. In the reaction mechanism, bromide is assumed to be coordinated with the zinc complex; however, our in situ studies indicate that dissociation of the zinc bromide complex occurred. The role of bromide could thus be either to act as nucleophiles for epoxide opening or to serve as an easy-leaving group, making free coordination sites at the zinc more accessible. This possibility is supported by the observation that iodide is even better than bromide [17,37]. We can also conclude that the mechanisms in the homogeneous and immobilized complexes are similar; however, more in situ studies are needed to unravel the complete mechanism.

5. Conclusions

High rates during the addition of CO_2 to propylene oxide were obtained using homogeneous zinc pyridine bromide catalysts, even without additional solvents. By immobilizing the active complex, this high activity was transferred to a heterogeneous catalyst, which also has high thermal stability because of the silica support. We have shown that the structure and activity of all intermediate stages of the immobilization can be followed step by step by both spectroscopic measurements and catalytic results. Variations in the structure were unraveled by XAS, and the change in catalytic activity could be related to a change in the coordination shell of the zinc and to the type of ligand in the catalyst. In situ XAS proved to be a well-suited technique for monitoring the structure of the catalyst under real reaction conditions, even at high pressure. Changes in the coordination sphere of the zinc and detachment of the bromide under reaction conditions were seen. Zinc is well immobilized. The observed presence of the bromide in the liquid-like reaction mixture not only provides insight into the mechanism, but also explains why bromide or similar ligands have been important in the design of active catalysts for the addition of CO_2 to epoxides. These findings indicate that when designing heterogeneous catalysts for this reaction, bromide can be used as a co-catalyst (as shown in this work), or the heterogenized catalyst can be modified by additional immobilization of the bromide as an onium salt.

Acknowledgments

The authors thank the Bundesamt für Energie (BFE) for financial support and the Swiss Norwegian Beamline (ESRF, Grenoble) and HASYLAB (DESY, Hamburg) for providing beam time. They also thank the beamline staff at SNBL (Herman Emerich, Wouter van Beek) and at beamline X1 (Mathias Hermann, Julia Wienold), as well as Matteo Caravati, for their support during the measurements. Finally, they thank Carsten Beck for the ICP-OES, Marek Maciejewski for the thermal analysis measurements, and Roland Mäder for the in situ cell construction.

References

[1] A. Behr, Angew. Chem., Int. Ed. 27 (1988) 661.
[2] H. Arakawa, M. Aresta, J.N. Armor, M.A. Barteau, E.J. Beckman, A.T. Bell, J.E. Bercaw, C. Creutz, E. Dinjus, D.A. Dixon, K. Domen, D.L. DuBois, J. Eckert, E. Fujita, D.H. Gibson, W.A. Goddard, D.W. Goodman, J. Keller, G.J. Kubas, H.H. Kung, J.E. Lyons, L.E. Manzer, T.J. Marks, K. Morokuma, K.M. Nicholas, R. Periana, L. Que, J. Rostrup-Nielson, W.M.H. Sachtler, L.D. Schmidt, A. Sen, G.A. Somorjai, P.C. Stair, B.R. Stults, W. Tumas, Chem. Rev. 101 (2001) 953.
[3] M. Aresta, E. Quaranta, Chem. Tech. 27 (1997) 32.
[4] A. Baiker, Appl. Organomet. Chem. 14 (2000) 751.
[5] A.A.G. Shaikh, S. Sivaram, Chem. Rev. 96 (1996) 951.
[6] I. Noriko, Japanese Patent JP 7,267,944 (1995), to Mitsubishi Chemistry Corporation.
[7] G. Rokicki, W. Kuran, Bull. Chem. Soc. Jpn. 57 (1984) 1662.
[8] G. Rokicki, W. Kuran, B. Pogorzelskamarciniak, Monatsh. Chem. 115 (1984) 205.
[9] N. Kihara, N. Hara, T. Endo, J. Org. Chem. 58 (1993) 6198.
[10] M. Ratzenhofer, H. Kisch, Angew. Chem. Int. Ed. 19 (1980) 317.
[11] A. Baba, T. Nozaki, H. Matsuda, Bull. Chem. Soc. Jpn. 60 (1987) 1552.
[12] S.A. Lermontov, S.V. Shkavrov, A.S. Lermontov, S.I. Zavorin, Russ. Chem. Bull. 47 (1998) 1607.
[13] D.J. Darensbourg, J.C. Yarbrough, J. Am. Chem. Soc. 124 (2002) 6335.
[14] R.L. Paddock, S.T. Nguyen, J. Am. Chem. Soc. 123 (2001) 11498.
[15] D.J. Darensbourg, S.J. Lewis, J.L. Rodgers, J.C. Yarbrough, Inorg. Chem. 42 (2003) 581.
[16] H.S. Kim, J.J. Kim, B.G. Lee, O.S. Jung, H.G. Jang, S.O. Kang, Angew. Chem. Int. Ed. 39 (2000) 4096.
[17] H.S. Kim, J.J. Kim, S.D. Lee, M.S. Lah, D. Moon, H.G. Jang, Chem. Eur. J. 9 (2003) 678.
[18] F.W. Li, C.G. Xia, L.W. Xu, W. Sun, G.X. Chen, Chem. Commun. (2003) 2042.
[19] H. Kawanami, A. Sasaki, K. Matsui, Y. Ikushima, Chem. Commun. (2003) 896.
[20] S. Fujita, B.M. Bhanage, Y. Ikushima, M. Shirai, K. Torii, M. Arai, Catal. Lett. 79 (2002) 95.
[21] H. Yasuda, L.N. He, T. Sakakura, J. Catal. 209 (2002) 547.
[22] H. Kawanami, Y. Ikushima, Chem. Commun. (2000) 2089.
[23] K. Yamaguchi, K. Ebitani, T. Yoshida, H. Yoshida, K. Kaneda, J. Am. Chem. Soc. 121 (1999) 4526.
[24] M. Tu, R.J. Davis, J. Catal. 199 (2001) 85.
[25] R. Srivastava, D. Srinivas, P. Ratnasamy, Catal. Lett. 89 (2003) 81.
[26] I.C. Chisem, J. Rafelt, M.T. Shieh, J. Chisem, J.H. Clark, R. Jachuck, D. Macquarrie, C. Ramshaw, K. Scott, Chem. Commun. (1998) 1949.
[27] M.H. Valkenberg, W.F. Holderich, Catal. Rev.-Sci. Eng. 44 (2002) 321.
[28] J.-D. Grunwaldt, M. Ramin, M. Rohr, A. Michailovski, G.R. Patzke, A. Baiker, Rev. Sci. Instr. 76 (2005) 054104.
[29] T. Ressler, J. Synchrotron Radiat. 5 (1998) 118.
[30] S.I. Zabinsky, J.J. Rehr, A. Ankudinov, R.C. Albers, M.J. Eller, Phys. Rev. B: Condens. Matter Mater. Phys. 52 (1995) 2995.
[31] K. Asakura, in: Y. Iwasawa (Ed.), X-Ray Absorption Fine Structure for Catalysts and Surfaces, World Scientific, Singapore–New Jersey–London–Hong Kong, 1996, p. 33.
[32] D.C. Koningsberger, R. Prins, TrAC, Trends Anal. Chem. 1 (1981) 16.
[33] V. Simonet, Y. Calzavara, J.L. Hazemann, R. Argoud, O. Geaymond, D. Raoux, J. Chem. Phys. 116 (2002) 2997.
[34] R.A. Sheldon, M. Wallau, I.W.C.E. Arends, U. Schuchardt, Acc. Chem. Res. 31 (1998) 485.
[35] J.A. Widegren, R.G. Finke, J. Mol. Catal. A: Chem. 198 (2003) 317.
[36] H. Bertagnolli, T. Engelhardt, B. Lengeler, Z. Phys. Chem. 155 (1987) 79.
[37] H.S. Kim, J.J. Kim, H.N. Kwon, M.J. Chung, B.G. Lee, H.G. Jang, J. Catal. 205 (2002) 226.
[38] X.B. Lu, H. Wang, R. He, J. Mol. Catal. A: Chem. 186 (2002) 33.
[39] R.L. Paddock, Y. Hiyama, J.M. McKay, S.T. Nguyen, Tetrahedron Lett. 45 (2004) 2023.
[40] I.W.C.E. Arends, R.A. Sheldon, Appl. Catal. A 212 (2001) 175.
[41] X.B. Lu, X.J. Feng, R. He, Appl. Catal. A 234 (2002) 25.